April 15, 1981

Electron momentum densities in disordered muffin-tin alloys

A. Bansil
Northeastern University

R. S. Rao
Northeastern University

P. E. Mijnarends
Netherlands Energy Research Foundation

L. Schwartz
Brandeis University

PHYSICAL REVIEW B VOLUME 23, NUMBER 8 15 APRIL 1981

Electron momentum densities in disordered muffin-tin alloys

A. Bansil and R. S. Rao
Department of Physics, Northeastern University, Boston, Massachusetts 02115

P. E. Mijnarends
Netherlands Energy Research Foundation, 1755 ZG Petten (N.H.), The Netherlanas

L. Schwartz
Department of Physics, Brandeis University, Waltham, Massachusetts 02154
(Received 4 August 1980)

The application of average t-matrix (ATA) and coherent potential (CPA) approximations to the calculation of average electron momentum density $\rho(\vec{p})$ in random muffin-tin alloys A_xB_{1-x} is considered. The necessary equations for the general matrix elements of the operators describing scattering by the CPA atom and also by an A or B atom embedded in the effective medium are derived. Various versions of the ATA for $\rho(\vec{p})$ are discussed. Several $\rho(\vec{p})$ curves calculated on the basis of the CPA and ATA in Cu_xNi_{1-x} are presented. These results are used to delineate the effects on $\rho(\vec{p})$ of self-consistency in the treatment of disorder.

I. INTRODUCTION

Much of the recent work concerning electronic structure of disordered metallic alloys has focused on the application of single-site approximations, and particularly the average t-matrix (ATA) and coherent potential (CPA) approximations, to the muffin-tin Hamiltonian. The application of these approximations to obtain the average electronic density of states $\rho(E)$ and associated spectral properties has reached a fair degree of maturity, although some difficult problems remain to be solved. The stage for a full theoretical development and discussion of other electronic properties [e.g., momentum densities, soft x-ray emission (or absorption) profiles, neutron scattering form factors, optical spectra, transport coefficients, etc.] would therefore appear to be clearly set. Our particular interest here is in the average electron momentum density, which is related to the measured positron-annihilation or Compton scattering profiles in random alloys.

In earlier publications,[1,2] we have presented the ATA formalism for $\rho(\vec{p})$ and applied it to Cu_xNi_{1-x}. In Ref. 3 a new version of the muffin-tin ATA for $\rho(E)$ (referred to as ATA2), which incorporates the physically important effects due to a single A or B impurity atom embedded in any given effective medium, was considered. A discussion of several aspects of the equilibrium electronic structure of Cu_xNi_{1-x} and Cu_xZn_{1-x} alloys on the basis of the muffin-tin CPA and ATA2 has also been reported.[4-6] The present article extends the ATA2 and CPA to the evaluation of momentum densities. Cu_xNi_{1-x} is used as an illustrative example, because we possess extensive relevant information (such as CPA solutions, complex energy bands, densities of states, etc.) on this system from our previous work.

New results reported in this paper are the following. (i) The muffin-tin CPA equation for the general matrix elements, $t^{CP}(p,p')$, of the CPA scatterer is derived (Sec. II A).[7] Our analysis shows that for the off-energy-shell elements (i.e., for p or $p' \neq \sqrt{E}$), this equation is not a nonlinear self-consistency condition (in contrast to the case of the on-energy-shell elements), but a simple linear equation in the unknowns. (ii) Explicit solutions for the (p,p') matrix elements of the scattering path operators, $\langle T^{\text{eff}}_{nn'}(p,p')\rangle_{0=A(B)}$ for a single $A(B)$ impurity embedded in any given effective medium are presented. (Note that these solutions are required for the calculation of the momentum densities whereas for evaluating the densities of states only the $p = p' = \sqrt{E}$ elements are necessary.) These results are used to derive and discuss ATA2 and CPA expressions for $\rho(\vec{p})$ in Sec. II B. (iii) Several CPA and ATA2 curves for $\rho(\vec{p})$ in Cu_xNi_{1-x} are presented in Sec. III. CPA and ATA2 values are compared with each other, and with earlier ATA [referred to as ATA1 (Ref. 2)] computations. Self-consistency in treating disorder is generally found to have rather little influence on the physically relevant quantity $\rho(\vec{p})$. (iv) Finally, the Appendix discusses how the various off- and on-energy-shell matrix elements occuring in the present multiple-scattering framework can be related to the solutions of the Schrödinger's equation within the A- and B-atom Wigner-Seitz cells. Such a reformulation of the theory is relevant for understanding charge distributions in alloys.

Effects of the positron wave function on the

momentum density are excluded from the scope of present work. It may be noted, nonetheless, that the incorporation of these effects within the framework of the independent particle model is a relatively straightforward proposition. This matter will be taken up in a subsequent study.

II. FORMALISM

A. General matrix elements of the coherent potential scatterer

We consider the substitutionally disordered binary alloy A_xB_{1-x} on the basis of the one-electron Hamiltonian

$$H = \frac{p^2}{2m} + \sum_n v_n^{A(B)}(r) . \tag{2.1}$$

Here the crystal potential is assumed to be given as the sum of nonoverlapping spherically symmetric muffin-tin potentials $v_n^{A(B)}(r) \equiv v^{A(B)}(|\vec{r} - \vec{R}_n|)$ centered on atomic sites $\{\vec{R}_n\}$. Because the alloy is assumed to be random the probability of any given site being occupied by an A (B) atom is equal to its fractional concentration x [or $y \equiv (1-x)$].

We analyze the average electronic spectrum of the alloy within the framework of the single-site approximation, which amounts to replacing the disordered alloy by an ordered crystal of appropriately chosen effective atoms. In the ATA, the effective atom is characterized by the scattering matrix $t^{\text{eff}} = \langle t \rangle \equiv xt^A + yt^B$. The CPA scatterer is more complicated and is determined by the physical requirement that, on the average, there be no scattering from a single A or B impurity embedded in the effective medium. More specifically,

$$x\bar{t}_n^A + y\bar{t}_n^B = 0 , \tag{2.2}$$

where

$$\bar{t}_n^{A(B)} = (v_n^{A(B)} - \sigma_n^{\text{CP}})[1 - G^{\text{CP}}(v_n^{A(B)} - \sigma_n^{\text{CP}})]^{-1} \tag{2.3}$$

is the t matrix for an $A(B)$ atom with respect to the effective medium. Here, σ_n^{CP} denotes the coherent potential (located on site n) and G^{CP} the CPA Green's function. Using (2.3) in (2.2) yields

$$\sigma^{\text{CP}} = xv^A + yv^B - (\sigma^{\text{CP}} - v^A)G^{\text{CP}}(\sigma^{\text{CP}} - v^B) , \tag{2.4}$$

where omission of the subscript n, by convention, implies $n = 0$. (This convention will be employed in the remainder of this article.) Equation (2.4) has been used extensively in the treatment of one- and two-band tight-binding model Hamiltonians. In the context of the muffin-tin Hamiltonian, however, it is more convenient to rewrite Eq. (2.2) in terms of the free-electron propagator G_0 and the scattering matrices t^A, t^B, and t^{CP} of the A, B, and CP atom, respectively. Using

$$\sigma^{\text{CP}} = t^{\text{CP}}(1 + G_0 t^{\text{CP}})^{-1} \tag{2.5}$$

and

$$v^{A(B)} = t^{A(B)}(1 + G_0 t^{A(B)})^{-1} \tag{2.6}$$

to eliminate v^A, v^B, and σ^{CP} in favor of the corresponding t matrices, Eq. (2.4) yields

$$t^{\text{CP}} = \langle t \rangle - (t^A - t^{\text{CP}})F^{\text{CP}}(t^B - t^{\text{CP}}) , \tag{2.7}$$

where

$$F^{\text{CP}} \equiv (1 + G_0 t^{\text{CP}})^{-1} G_0 (T^{\text{CP}} - t^{\text{CP}}) G_0 (1 + t^{\text{CP}} G_0)^{-1} , \tag{2.8}$$

and T^{CP} is the total scattering operator for the CP medium related to G^{CP} by

$$G^{\text{CP}} = G_0 + G_0 T^{\text{CP}} G_0 . \tag{2.9}$$

With the decomposition

$$T = \sum_{n,n'} T_{nn'} \tag{2.10}$$

of T in terms of the path operators $T_{nn'}$, the operator F can be rewritten as

$$F = G_0 \sum_{n \neq 0, n' \neq 0} T_{nn'} G_0 . \tag{2.11}$$

[Superscripts CP are suppressed in Eqs. (2.10) and (2.11) because these are operator identities.] Specializing to the muffin-tin Hamiltonian, we write G_0 and the various scattering matrices in the angular momentum representation. Thus

$$t^{\text{CP}}(\vec{p}, \vec{p}') = (4\pi)^2 \sum_{LL'} Y_L(\hat{p}) t_{LL'}^{\text{CP}}(p, p') Y_{L'}(\hat{p}') , \tag{2.12}$$

with similar equations for $t^A(\vec{p}, \vec{p}')$ and $t^B(\vec{p}, \vec{p}')$, and

$$G_0(\vec{r} - \vec{r}' - \vec{R}_n) = \sum_{LL'} Y_L(\hat{r}) j_l(\kappa r) B_{0n}^{LL'} j_{l'}(\kappa r') Y_{L'}(\hat{r}') . \tag{2.13}$$

Here $\kappa \equiv \sqrt{E}$, $L \equiv (l,m)$ is a composite angular momentum index, and $Y_L(\hat{x})$ is the real spherical harmonic associated with direction $\hat{x}$. B_{0n} is the matrix of lattice Fourier transforms of the usual Korringa-Kohn-Rostoker (KKR) structure functions $B_{\vec{k}}(E)$. By straightforward manipulations Eq. (2.7) can be cast into the form[8]

$$t^{\text{CP}}(p, p') = \langle t(p, p') \rangle - [t^A(p, \kappa) - t^{\text{CP}}(p, \kappa)]F^{\text{CP}} \times [t^B(\kappa, p') - t^{\text{CP}}(\kappa, p')] \tag{2.14}$$

with F^{CP} given by a Brillouin-zone summation

$$F^{\text{CP}} \equiv \frac{1}{N} \sum_{\vec{k}} B_{\vec{k}}(1 - \tau_{\text{CP}} B_{\vec{k}})^{-1} . \tag{2.15}$$

Equation (2.14) and (2.15) are to be understood

as matrix equations in (L, L') space. Here, $\tau_{CP} \equiv t^{CP}(\kappa, \kappa)$ denotes the on-shell elements of t^{CP}.

Equation (2.14) permits the calculation of arbitrary matrix elements of the CP scatterer and for $p = p' = \kappa$, it reduces to the usual CPA self-consistency condition. Note that for half-off-shell elements $t^{CP}(p, \kappa)$ [or $t^{CP}(\kappa, p)$], (2.14) is *not* a self-consistency condition, but a simple linear equation in the unknowns. Once τ_{CP} is obtained, all other elements of the CP scatterer are computed easily in terms of τ_{CP}; no additional nonlinear equations need be solved. It is clear then that the average one-electron properties (in particular, momentum densities, real space charge densities, and Bloch spectral functions) of the muffin-tin alloy in the CPA are determined unambiguously via the solutions of the usual CPA equation, without recourse to any further approximations.[9] (See the Appendix for a discussion). This is also true of physical quantities which involve the properties of a single A or B atom embedded in the CPA medium (e.g., the A and B component charge densities).

B. Average momentum density in ATA and CPA

The average electron momentum density in an effective medium is given by

$$\rho^{\text{eff}}(\vec{p}) = \int_{-\infty}^{E_F} dE\, \rho^{\text{eff}}(\vec{p}, E), \tag{2.16}$$

where E_F is the Fermi energy, and the spectral momentum density $\rho^{\text{eff}}(\vec{p}, E)$ is related to the ensemble-averaged Green's function, $G^{\text{eff}}(\vec{p}, \vec{p}; E) \equiv G^{\text{eff}}(\vec{p}, E)$ by

$$\rho^{\text{eff}}(\vec{p}, E) = -\pi^{-1}\text{Im}G^{\text{eff}}(\vec{p}, E^+) . \tag{2.17}$$

$G^{\text{eff}}(\vec{p}, E)$ can be written in terms of the one-site-restricted average Green's function

$$G^{\text{eff}}(\vec{p}, E) = x\langle G(\vec{p}, E)\rangle^{\text{eff}}_{0=A} + y\langle G(\vec{p}, E)\rangle^{\text{eff}}_{0=B} . \tag{2.18}$$

$\langle G(\vec{p}, E)\rangle^{\text{eff}}_{0=A(B)}$ may be evaluated approximately on physical grounds placing an $A(B)$ atom at the zeroth site in the effective medium, i.e., by solving the single-impurity problem. Note, however, that the value of $G^{\text{eff}}(\vec{p}, E)$ computed for a given effective medium t^{eff} with such approximate $\langle G\rangle^{\text{eff}}_{0=A}$ and $\langle G\rangle^{\text{eff}}_{0=B}$ values will be equal to that obtained by placing t_{eff} at every site in the crystal only if $t_{\text{eff}} = t_{CP}$.[11] In this sense, the CPA incorporates the properties of a single A or B impurity embedded in the effective medium. With this motivation, we have recently proposed a version[3] of the muffin-tin ATA (referred to as ATA2 in Ref. 3, which includes the physically important single-impurity effects, yields the CPA for $t^{\text{eff}} = t_{CP}$) and possesses other desirable features.

To develop an expression for the momentum density in spirit of the ATA2 and in the CPA, we require the momentum matrix elements $\langle T(p, p'; E)\rangle^{\text{eff}}_{0=A(B)}$ of the total scattering operator for a single $A(B)$ atom placed in an effective medium.

When restricted averages of both sides of Eq. (2.10) are taken, we have

$$\langle T^{\text{eff}}\rangle_{0=A(B)} = \sum_{nn'} \langle T^{\text{eff}}_{nn'}\rangle_{0=A(B)} , \tag{2.19}$$

where the path operators $\langle T^{\text{eff}}_{nn'}\rangle_{0=A(B)}$ satisfy[12]

$$\langle T^{\text{eff}}_{nn}\rangle_{0=A(B)} = [t^{\text{eff}}_n + (t^A_n - t^{\text{eff}}_n)\delta_{n0}] \times \left(\delta_{nn'} + G_0 \sum_{m\neq n} \langle T^{\text{eff}}_{mn'}\rangle_{0=A(B)}\right). \tag{2.20}$$

Substitution of

$$\langle T^{\text{eff}}_{nn'}(\vec{p}, \vec{p}')\rangle_{0=A(B)} = \sum_{LL'} Y_L(\hat{p})\langle T^{\text{eff}}_{nn'}(p, p')\rangle^{LL'}_{0=A(B)} Y_{L'}(\hat{p}') \tag{2.21}$$

in (2.20) yields a matrix equation in (L, L') space whose solution is easily obtained by a Fourier transform of the lattice coordinates (n, n'). The final result is[13]

$$\begin{aligned}\langle T^{\text{eff}}_{nn'}(p, p')\rangle_{0=A(B)} = &\{t^{\text{eff}}_n(p, p') + [t^{A(B)}_n(p, p') - t^{\text{eff}}_n(p, p')]\delta_{n0}\}\,\delta_{nn'} + \{t^{\text{eff}}_n(p, \kappa) + [t^{A(B)}_n(p, \kappa) - t^{\text{eff}}_n(p, \kappa)]\delta_{n0}\} \\ &\times \Big(-\delta_{nn'} + \tau^{-1}_{\text{eff}} T^{\text{eff}}_{nn'})\tau^{-1}_{\text{eff}} t^{\text{eff}}(\kappa, p') + (-\delta_{n0} + \tau^{-1}_{\text{eff}} T^{\text{eff}}_{n0})\Delta^{\text{eff}}_{A(B)} \frac{1}{1 - T^{\text{eff}}_{00}\Delta^{\text{eff}}_{A(B)}} T^{\text{eff}}_{0n'}\tau^{-1}_{\text{eff}} t^{\text{eff}}(\kappa, p') \\ &+ (-\delta_{n0} + \tau^{-1}_{\text{eff}} T^{\text{eff}}_{n0}) \frac{1}{1 - \Delta^{\text{eff}}_{A(B)} T^{\text{eff}}_{00}} [\tau^{-1}_{A(B)} t^{A(B)}(\kappa, p') - \tau^{-1}_{\text{eff}} t^{\text{eff}}(\kappa, p')]\delta_{0n'}\Big) ,\end{aligned} \tag{2.22}$$

where $T^{\text{eff}}_{nn'}$ is given by the Brillouin-zone summation

$$T^{\text{eff}}_{nn'} = \frac{1}{N}\sum_{\vec{k}} e^{i\vec{k}\cdot(\vec{R}_n - \vec{R}_{n'})}\left(\frac{1}{\tau^{-1}_{\text{eff}} - B_{\vec{k}}}\right) \tag{2.23}$$

and

$$\Delta^{\text{eff}}_{A(B)} = \tau^{-1}_{\text{eff}} - \tau^{-1}_{A(B)} . \tag{2.24}$$

As discussed in Ref. 3, we are interested in the contribution

$$\langle T_0^{\rm eff}(p,p)\rangle \equiv \sum_{n'} \langle T_{0n'}^{\rm eff}(p,p)\rangle \tag{2.25}$$

of the zeroth site to the total scattering operator. Using (2.25) and (2.24) this may be written as

$$\langle T_0^{\rm eff}(p,p)\rangle = x\langle T_0^{\rm eff}(p,p)\rangle_{0\in A} + y\langle T_0^{\rm eff}(p,p)\rangle_{0\in B} \tag{2.26}$$

$$= F_1 + F_2 + F_3 + F_4 , \tag{2.27}$$

where

$$F_1 = \langle t(p,p)\rangle - [xt^A(p,\kappa)\tau_A^{-1}t^A(\kappa,p) + yt^B(p,\kappa)\tau_B^{-1}t^B(\kappa,p)] , \tag{2.28a}$$

$$F_2 = x[t^A(p,\kappa)\tau_A^{-1} - t^{\rm eff}(p,\kappa)\tau_{\rm eff}^{-1}]T_{00}^{\rm eff}\frac{1}{1-\Delta_A^{\rm eff}T_{00}^{\rm eff}}[\tau_A^{-1}t^A(\kappa,p) - \tau_{\rm eff}^{-1}t^{\rm eff}(\kappa,p)]$$

$$+ y[t^B(p,\kappa)\tau_B^{-1} - t^{\rm eff}(p,\kappa)\tau_{\rm eff}^{-1}]T_{00}^{\rm eff}\frac{1}{1-\Delta_B^{\rm eff}T_{00}^{\rm eff}}[\tau_B^{-1}t^B(\kappa,p) - \tau_{\rm eff}^{-1}t^{\rm eff}(\kappa,p)] , \tag{2.28b}$$

$$F_3 = t^{\rm eff}(p,\kappa)\tau_{\rm eff}^{-1}T_{00}^{\rm eff}\left(\frac{x}{1-\Delta_A^{\rm eff}T_{00}^{\rm eff}}[\tau_A^{-1}t^A(\kappa,p) - \tau_{\rm eff}^{-1}t^{\rm eff}(\kappa,p)] + \frac{y}{1-\Delta_B^{\rm eff}T_{00}^{\rm eff}}[\tau_B^{-1}t^B(\kappa,p) - \tau_{\rm eff}^{-1}t^{\rm eff}(\kappa,p)]\right) , \tag{2.28c}$$

and

$$F_4 = \left(xt^A(p,\kappa)\tau_A^{-1}\frac{1}{1-T_{00}^{\rm eff}\Delta_A^{\rm eff}} + yt^B(p,\kappa)\tau_B^{-1}\frac{1}{1-T_{00}^{\rm eff}\Delta_B^{\rm eff}}\right)\frac{1}{\tau_{\rm eff}^{-1}-B_{\vec{p}}}\tau_{\rm eff}^{-1}t^{\rm eff}(\kappa,p) . \tag{2.28d}$$

Equations (2.25) through (2.28) provide[3] an expression for $\rho(\vec{p})$ which incorporates single-impurity effects. However, these equations must be modified to ensure an exact cancellation of the free-electron poles in $\rho^{\rm eff}(\vec{p},E)$ for arbitrary effective medium. (This cancellation is automatic for the case $t^{\rm eff}=t_{\rm CP}$.) For $\rho^{\rm eff}(\vec{p},E)$ to vary smoothly as $p\to\kappa$, two conditions must be satisfied[1]: (i) the terms independent of the structure functions $B_{\vec{p}}$ must vanish at least as fast as $(E-p^2)^2$, and (ii) $B_{\vec{p}}$-dependent term involving the inverse matrix $(\tau_{\rm eff}^{-1}-B_{\vec{p}})^{-1}$ should diverge as $(E-p^2)^{-1}$. We discuss these conditions in turn.

Of the $B_{\vec{p}}$-independent terms (i.e., F_1, F_2, and F_3), F_1 and F_2 obviously vary as $(E-p^2)^2$, but $F_3\sim(E-p^2)$. While F_3 vanishes rigorously in the CPA, it turns out that in the general case it is difficult to ensure a proper behavior for F_3 as $p\to\kappa$, and therefore we have dropped the contribution F_3 from our final expression for $\rho^{\rm eff}(\vec{p},E)$. For the $B_{\vec{p}}$-dependent term F_4, we use the replacement

$$(1-T_{00}^{\rm eff}\Delta_A^{\rm eff})^{-1} \to \frac{1}{x}(\tau_{\rm eff}^{-1}-\tau_B^{-1})(\tau_A^{-1}-\tau_B^{-1})^{-1} , \tag{2.29}$$

(with a similar relation with the interchange $A\leftrightarrow B$) in the prefactor enclosed in the large parentheses in expression (2.28d) to obtain

$$\tilde{F}_4 = \left(t_A(p,\kappa)\tau_A^{-1}\frac{1}{\tau_A^{-1}-\tau_B^{-1}}(\tau_{\rm eff}^{-1}-\tau_B^{-1}) + t_B(p,\kappa)\tau_B^{-1}\frac{1}{\tau_B^{-1}-\tau_A^{-1}}(\tau_{\rm eff}^{-1}-\tau_A^{-1})\right)\frac{1}{\tau_{\rm eff}^{-1}-B_{\vec{p}}}\tau_{\rm eff}^{-1}t_{\rm eff}(\kappa,p) . \tag{2.30}$$

The replacement (2.29) is exact in the CPA and was also used previously in connection with ATA2.[3] Our final result for $\rho^{\rm eff}(\vec{p},E)$ is

$$\rho^{\rm eff}(\vec{p},E) = -\frac{1}{\pi}\,{\rm Im}\left(\frac{1}{E+i0^+-p^2} + \frac{(4\pi)^2N}{(E+i0^+-p^2)^2}\sum_{LL'}Y_L(\hat{p})(F_1+F_2+\tilde{F}_4)_{LL'}Y_{L'}(\hat{p})\right) , \tag{2.31}$$

with F_1, F_2, and $\tilde{F}_4$ given, respectively, by Eqs. (2.28a), (2.28b), and (2.30).

In the preceding discussion of the free-electron poles, we have assumed implicitly that for $p\to\kappa$, $t^{\rm eff}(p,p)$, $t^{\rm eff}(p,\kappa)$, and $t^{\rm eff}(\kappa,p)\to t^{\rm eff}(\kappa,\kappa)\equiv\tau^{\rm eff}$, and also that $t_{A(B)}(p,\kappa)\to t_{A(B)}(\kappa,\kappa)$. The question of how to ensure the proper limiting behavior for $t_{A(B)}(p,\kappa)$ was considered in Ref. 2. The easiest method of ensuring this behavior for $t^{\rm eff}(p,p')$ is to evaluate the matrix elements for $p=p'=\kappa$, as

well as for p or $p' \neq \kappa$ via equations which *explicitly* possess the proper limiting behavior. This can be accomplished by a few straightforward manipulations on the CPA equation (2.14). The relevant (matrix) equation is

$$t^{\text{eff}}(p,p') = \langle t(p,p') \rangle - [t_A(p,\kappa) - \langle t(p,\kappa) \rangle] M^{\text{eff}} \times [t_B(\kappa,p') - \langle t(\kappa,p') \rangle], \quad (2.32)$$

where

$$M^{\text{eff}} \equiv \frac{1}{1 - F^{\text{eff}}(\tau_B - \tau_{\text{eff}})} F^{\text{eff}} \frac{1}{1 - (\tau_A - \tau_{\text{eff}}) F^{\text{eff}}}, \quad (2.33)$$

and

$$F^{\text{eff}} \equiv \frac{1}{N} \sum_{\vec{q}} B_{\vec{q}} \frac{1}{1 - \tau_{\text{eff}} B_{\vec{q}}}. \quad (2.34)$$

We emphasize that Eq. (2.32) is not meant to be solved for t^{eff}. Instead, given the values of τ_{eff} and F^{eff} (obtained during the course of solving the CPA equation), Eq. (2.32) *determines* new values of $t^{\text{eff}}(p,p')$, which are guaranteed to reduce properly in the limit p or $p' \to \kappa$. Finally we note that by repeated use of the CPA equation, it can be shown that

$$(F_1 + F_2 + \tilde{F}_4)_{\text{CPA}} = t^{\text{CP}}(p,p) - t^{\text{CP}}(p,\kappa)\tau_{\text{CP}}^{-1} t^{\text{CP}}(\kappa,p) + t^{\text{CP}}(p,\kappa)\tau_{\text{CP}}^{-1}\left(\frac{1}{\tau_{\text{CP}}^{-1} - B_{\vec{p}}}\right) \times \tau_{\text{CP}}^{-1} t^{\text{CP}}(\kappa,p). \quad (2.35)$$

The substitution of (2.35) in Eq. (2.31) yields an expression for $\rho^{\text{CP}}(\vec{p},E)$, which can also be obtained directly by placing a CP atom at every lattice site in the alloy. This shows that (2.33) reduces properly in the case $t^{\text{eff}} = t^{\text{CP}}$. By contrast, as already noted, for $t^{\text{eff}} = \langle t \rangle$ Eq. (2.31) does not reduce to the usual ATA (i.e., placing a $\langle t \rangle$ atom on every lattice site), but represents a new version of the ATA for momentum densities in any given effective medium.

III. ILLUSTRATIVE RESULTS

Spectral momentum densities $\rho(\vec{p},E)$ for two different versions of the ATA and the CPA are presented in Figs. 1 and 2.[14] A general $\vec{k}$ point in the Brillouin zone (with no particular symmetry properties) is considered. The ATA1 (filled dots) and ATA2 (dashed) values[15] of normal as well as umklapp contributions to $\rho(\vec{p},E)$ are seen to be very close to each other. This may be understood qualitatively by recalling that these two versions of the ATA differ in that the ATA2 incorporates the effects of a single A or B impurity, while ATA1 does not. Since impurity states tend to be localized in real space, their effects are expected to be delocalized in momentum space.[16] Indeed, we find that the net contribution from the F_1 and F_2 terms [cf. Eq. (2.31)] is 2 to 3 orders of magnitude smaller than the plotted values of $\rho(\vec{p},E)$.

Turning to the comparison of CPA and ATA2 (or ATA1) in Fig. 1, we see that a self-consistent treatment of disorder causes two characteristic effects on $\rho(\vec{p},E)$: (i) the structure associated

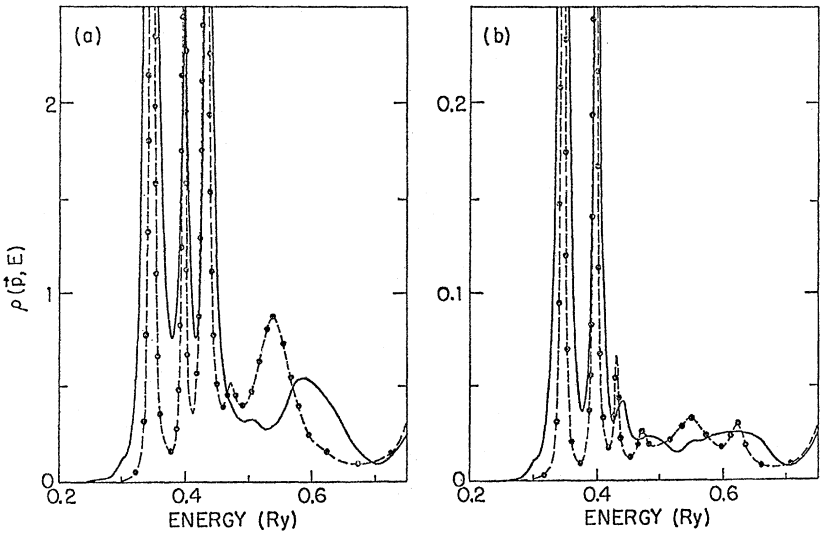

FIG. 1. Spectral momentum density $\rho(\vec{p},E)$ for ATA1 (filled circles), ATA2 (dashed) (Ref. 15), and CPA (solid) in $Cu_{0.75}Ni_{0.25}$ as a function of energy at (a) $\vec{p} = \vec{k}_0 \equiv (0.166, 0.415, 0.664)\ (2\pi/a)$, and (b) $\vec{p} = \vec{k}_0 + \vec{K}_{111}$ (1.166, 1.415, 1.664) $(2\pi/a)$, where $a = 6.8309$ a.u. is the Cu lattice constant. (Note that the vertical scales on the right-hand-side set of figures are ten times smaller than those for the left-hand side.)

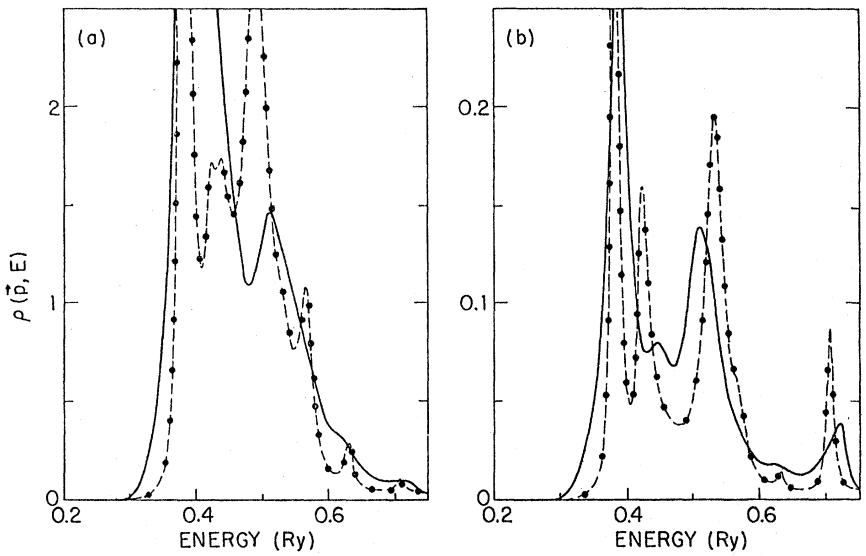

FIG. 2. Same as Fig. 1 except that this figure is for $Cu_{0.25}Ni_{0.75}$ (Ref. 17).

with the Ni-derived *d* states (in the range 0.45 to 0.65 Ry) is considerably broadened and shifted to higher energies, and (ii) the peaks arising from the Cu-like *d* states (in the range 0.3 to 0.45 Ry) are broadened and relatively less shifted. Similar effects were discussed in connection with the Bloch spectral density and the density of states in Ref. 5. They are a manifestation of the generally larger damping of states given by the CPA scatterer and of the *d-d* repulsion, which shifts the Ni *d* resonance to higher energies in the Cu-rich alloy. Much of the preceding discussion is also applicable to $Cu_{0.25}Ni_{0.75}$ considered in Fig. 2 and to other alloy compositions that we have studied (not shown). Note that in the Ni-rich regime the Cu-impurity resonance in the ATA (the structure around 0.43 Ry in Fig. 2) is completely smeared out in the CPA in Fig. 2(a), and only a hint of this structure remains in the CPA umklapp curve of Fig. 2(b).

Figure 3 compares the momentum density in CPA and ATA along the ⟨110⟩ direction. The differences between the two curves are not discernible on the scale of the figure. We find similar results along other directions in the Brillouin zone (not shown). In this connection, Fig. 4 is particularly interesting. As discussed in Ref. 2, the dip in $\rho(\vec{p})$ [appearing around (112) point] is associated with the fact that, as the Ni concentration increases from 50% to 75%, the Fermi energy falls below the top of the Ni *d* bands and, as a

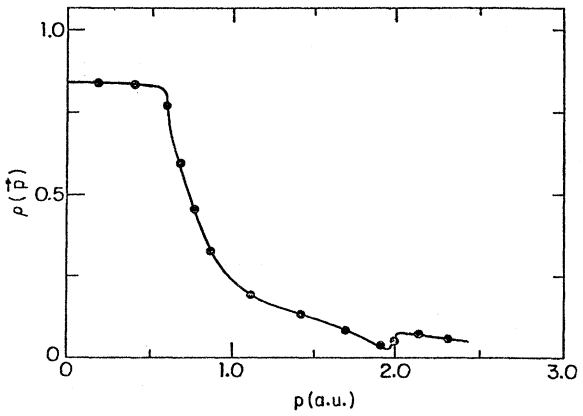

FIG. 3. ATA2 (solid) and CPA (filled circles) momentum density $\rho(\vec{p})$ along ⟨110⟩ in $Cu_{0.75}Ni_{0.25}$.

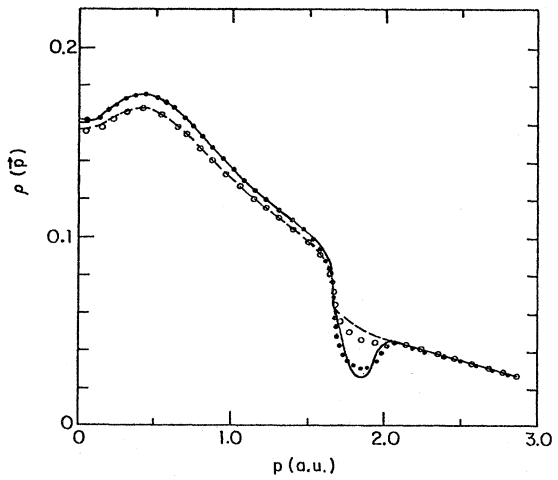

FIG. 4. ATA2 and CPA momentum densities $\rho(\vec{p})$ in $Cu_{0.25}Ni_{0.75}$ (solid, ATA; filled circles, CPA) and $Cu_{0.5}Ni_{0.5}$ (dashed, ATA; unfilled circles, CPA) along the line joining the points (1,1,0) and (1,1,3) in momentum space (Ref. 17).

result, hole ellipsoids appear around the symmetry point X in the Brillouin zone. Figure 4 shows that even such a delicate feature of $\rho(\vec{p})$ is influenced by only a small amount in going from ATA to CPA.

Although the spectral momentum density $\rho(\vec{p},E)$ differs significantly between the CPA and ATA (see Figs. 1 and 2), the momentum density $\rho(\vec{p})$ on the basis of the two approximations shows a striking similarity (see Figs. 3 and 4). This effect can be understood qualitatively in terms of Eq. (2.16) which defines $\rho(\vec{p})$ in terms of $\rho(\vec{p},E)$. In this context, two points are noteworthy: (i) A peak in $\rho(\vec{p},E)$ which is well below E_F will yield an approximately similar contribution to $\rho(\vec{p})$ and, therefore, changes in its precise location in energy and width are not important; (ii) the values of E_F in ATA and CPA differ in general in such a manner as to tend to compensate for any overall movement of energy levels across E_F. For these reasons, we believe that the present insensitivity of $\rho(\vec{p})$ to the use of self-consistency in the treatment of disorder can be expected to hold more generally in transition- and noble-metal alloys.

This work was supported in part by National Science Foundation Grant No. DMR79-02600 and by Grant No. DMR77-27249.

APPENDIX

Our purpose is to show how the real-space matrix elements of various quantities occurring in the theory can be obtained. As noted earlier, such a transformation is particularly relevant for a discussion of charge densities in the alloy. For illustrative purposes, we consider the average CPA Green's function G^{CP}.

We use the form (2.32) of the CPA equation in the coordinate representation

$$t^{CP}(r,r') = \langle t(r,r')\rangle - [t_A(r,\kappa) - \langle t(r,\kappa)\rangle]M^{CP} \times [t_B(\kappa,r') - \langle t(\kappa,r')\rangle], \quad \text{(A1)}$$

where $\vec{r}$ and $\vec{r}'$ are confined to the cell at the zeroth site and M^{CP} is defined via (2.33) with $\tau_{eff} = \tau_{CP}$. Our results are best formulated in terms of the real solutions $R_l^{A(B)}(r)$ of the radial Schrödinger's equation in the $A(B)$ muffin-tin sphere and the associated scattering solution

$$\psi_l^{A(B)}(r) \equiv -\kappa\tau_l^{A(B)} R_l^{A(B)}(r) \quad \text{(A2a)}$$

$$= j_l(\kappa r) + \int dr_1 r_1^2 g_l(r,r_1) t_l^{A(B)}(r_1,r), \quad \text{(A2b)}$$

where $g_l(r,r') = -i\kappa j_l(\kappa r_<) h_l(\kappa r_>)$ is the angular momentum decomposition of the free electron propagator and $\psi_l^{A(B)}$ is normalized (for $r \geq r_m$) to

$$\psi_l^{A(B)}(r) = e^{i\delta_l^{A(B)}}[j_l(\kappa r)\cos\delta_l^{A(B)} - n_l(\kappa r)\sin\delta_l^{A(B)}]. \quad \text{(A3)}$$

To evaluate the site-diagonal matrix elements $\langle \vec{r}+\vec{R}_n | G^{CP} | \vec{r}'+\vec{R}_n\rangle$, we employ the identity

$$G^{CP} = G_0 + G_0 t_n^{CP} G_0 + G_0(1 + t_n^{CP} G_0) \sum_{i\neq n, j\neq n} T_{ij}^{CP}(1 + G_0 t_n^{CP}) G_0. \quad \text{(A4)}$$

On substitution from (A1), (A2), and (A3), the first two terms on the right-hand side of (A4) yield

$$\langle \vec{r}+\vec{R}_n | (G_0 t_n^{CP} G_0) | \vec{r}'+\vec{R}_n\rangle = \sum_L Y_L(\hat{r})\{\langle G_l(r,r')\rangle - [\psi_l^A(r) - \langle\psi_l(r)\rangle]M_L^{CP}[\psi_l^B(r') - \langle\psi_l(r')\rangle]\} Y_L(\hat{r}'), \quad \text{(A5)}$$

with $\langle G_l\rangle \equiv xG_l^A + yG_l^B$ and $\langle\psi_l\rangle \equiv x\psi_l^A + y\psi_l^B$. Similarly, the last term on the right side of (A4) gives

$$\left\langle \vec{r}+\vec{R}_n \middle| G_0(1 + t_n^{CP} G_0) \sum_{i\neq n, j\neq n} T_{ij}^{CP}(1 + G_0 t_n^{CP}) G_0 \middle| \vec{r}'+\vec{R}_n \right\rangle = \sum_{LL'} Y_L(\hat{r})\{\langle\psi_l(r)\rangle - [\psi_l^A(r) - \langle\psi_l(r)\rangle]M_L^{CP}(\tau_l^A - \langle\tau_l\rangle)\} F_{LL'}^{CP} \times \{\langle\psi_{l'}(r')\rangle - (\tau_{l'}^A - \langle\tau_{l'}\rangle)M_{L'}^{CP}[\psi_{l'}^A(r') - \langle\psi_{l'}(r')\rangle]\} Y_{L'}(\hat{r}'), \quad \text{(A6)}$$

where F^{CP} was defined previously by Eq. (2.15). In deriving (A6), we have used the identity

$$h_l(\kappa|\vec{r} - \vec{R}_n|) Y_L(\vec{r} - \vec{R}_i) = \sum_{L_1} B_{mn}^{LL_1} j_{l_1}(\kappa r) Y_{L_1}(\hat{r}), \quad \text{(A7)}$$

where B_{nm} are the KKR structure functions [cf. Eq. (2.13)].[18] If the A- and B-atom phase shifts for $l \geq 3$ are neglected, the matrix F^{CP} is diagonal, and when (A5) and (A6) are combined, the local charge density in the cell at site n takes the form

$$\rho^{CP}(\vec{r},E) = \pi^{-1}\,\mathrm{Im}\,\langle \vec{r}+\vec{R}_n | G^{CP} | \vec{r}+\vec{R}_n\rangle = \pi^{-1} E\,\mathrm{Im}\sum_L Y_L(\hat{r})[xR_l^A(r)C_L^A R_l^A(r) + yR_l^B(r)C_L^B R_l^B(r)] Y_L(\hat{r}), \quad \text{(A8)}$$

where

$$C_L^{A(B)} = T_L\{1+[(\tau_l^{A(B)})^{-1} - (\tau_L^{CP})^{-1}]\,T_L\}^{-1} \tag{A9a}$$

$$\equiv T_L D_L^{A(B)} \tag{A9b}$$

and

$$T_L \equiv \tau_L^{CP} + \tau_L^{CP} F_L^{CP} \tau_L^{CP}. \tag{A10}$$

It may be noted that our CPA charge density (A8) is equivalent to the corresponding expression derived in Ref. 10. The identification of individual terms in (A8) as A- and B-component charge densities by Faulkner and Stocks[10] appears reasonable. However, as emphasized in Ref. 3, differences between various approximate methods of calculating component charge densities (and other physical properties) for muffin-tin alloys are likely to be smaller than the uncertainties inherent in the present *ab initio* framework. Therefore, such differences are of little physical consequence.

As emphasized elsewhere,[19] to calculate the Bloch spectral density, we require the non-site-diagonal matrix elements $\langle \vec{r}+\vec{R}_n|\, G^{CP}|\, \vec{r}'+\vec{R}_m\rangle$ $(n \neq m)$. To evaluate these quantities, we use the operator identity

$$G^{CP} = (1+G_0 t_n^{CP})\left(G_0 + G_0 \sum_{i\neq n, j\neq m} T_{ij}^{CP} G_0\right)(1+t_m^{CP} G_0). \tag{A11}$$

Proceeding as in the derivation of (A8), we find

$$\mathrm{Im}\langle \vec{r}+\vec{R}_n|G^{CP}|\,\vec{r}'+\vec{R}_m\rangle = E\ \mathrm{Im}\sum_{LL'} Y_L(\hat{r})\left(\sum_{i,j} c_i c_j R_l^{(i)}(r) P_{LL'}^{(ij)}(n-m) R_{l'}^{(j)}(r')\right) Y_{L'}(\hat{r}'), \tag{A12}$$

where the indices i and j are summed over the atomic species A, B and $c_A \equiv x$, $c_B \equiv y$. [Thus, the term in large parentheses in (A12) involves a sum of four terms.] The quantities $P_{LL'}^{(ij)}(n-m)$ are defined by

$$P_{LL'}^{(ij)}(n-m) = D_L^{(i)}\, T_{nm}^{CP}\, D_{L'}^{(j)}, \tag{A13}$$

with $D_L^{A(B)}$ given by (A9b). Equations (A8) and (A12) are sufficient to derive, for example, the CPA Bloch spectral density of Ref. 10.

---

[1] P. E. Mijnarends and A. Bansil, Phys. Rev. B 13, 2381 (1976).

[2] P. E. Mijnarends and A. Bansil, Phys. Rev. B 19, 2912 (1979).

[3] A. Bansil, Phys. Rev. B 20, 4025 (1979).

[4] A. Bansil, Phys. Rev. Lett. 41, 1670 (1978).

[5] A. Bansil, Phys. Rev. B 20, 4035 (1979).

[6] G. M. Stocks, W. M. Temmerman, and B. L. Gyorffy, Phys. Rev. Lett. 41, 339 (1978); W. M. Temmerman, B. L. Gyorffy, and G. M. Stocks, J. Phys. F 8, 2461 (1978). These publications consider the Bloch spectral function $\tilde{A}(\vec{k}, E)$ and not the momentum density $\rho(\vec{p}, E)$. We emphasize that the function $\rho(\vec{p}, E)$ contains information concerning the momentum distribution of various $\vec{k}$ states (which are Bloch wave functions in a perfect crystal) in the system. This unique information is lost (see Ref. 1) in the construction of $\tilde{A}(\vec{k}, E) \equiv \sum_{\vec{K}_n} \rho(\vec{k}+\vec{K}_n, E)$.

[7] This equation was used by Schwartz and Bansil [Phys. Rev. B 21, 4322 (1980)] in a different context (see footnote 20 of this reference).

[8] Since the expression (2.11) entails the exclusions $n \neq 0$ and $n' \neq 0$, the multiple-scattering expansion of the second term on the right side of Eq. (2.7) will not involve any terms in which two successive scatterings take place from the *same* site. As a result, F^{CP} [cf. Eq. (2.15)] depends only on the on-shell elements τ_{CP} and the dependence on p, p' in Eq. (2.14) occurs in a relatively straightforward manner. [See also the derivation of Eq. (A5) of the review article by H. Ehrenreich and L. Schwartz, in *Solid State Physics*, edited by H. Ehrenreich, F. Seitz, and D. Turnbull (Academic, New York, 1976), Vol. 31.]

[9] In particular, there is no need to invoke further decouplings [see Eq. (2.41) of Faulkner and Stocks (Ref. 10)].

[10] J. S. Faulkner and G. M. Stocks, Phys. Rev. B 21, 3222 (1980).

[11] In fact, the statement that Eq. (2.18) be valid with $\langle G(\vec{p}, E)\rangle_{0=A(B)}^{\mathrm{eff}}$ obtained by solving the single-impurity problem is equivalent to the CPA condition (2.7).

[12] B. L. Gyorffy, Phys. Rev. B 5, 2382 (1972).

[13] We note in passing that the off-shell elements of the CP scatterer may also be obtained via the condition[11]

$$[x\langle T_{nn'}^{CP}(p,p')\rangle_{0=A(B)} + y\langle T_{mn'}^{CP}(p,p')\rangle_{0=A(B)} = T_{mn'}^{CP}(p,p')].$$

Indeed, with the solution (2.22) it can be shown that the above equation leads to the CPA condition [cf. Eq. (2.14)] derived in Sec. II A.

[14] $\rho(\vec{p}, E)$ and $\rho(\vec{p})$ curves presented in Ref. 2 are in error by a constant factor of $(a/2\pi)^4 = 1.397$. Accordingly, the present ATA1 values are smaller than the corresponding values of Ref. 2 by a factor of 1.397.

[15] More specifically, ATA1 refers to the use of Eq. (2.2) of Ref. 2. [This can be shown to be equivalent of

setting $t^{\text{eff}} = \langle t \rangle$ and $T_{00}^{\text{eff}} = \langle \tau \rangle$ in Eq. (2.31).] ATA2 is defined by Eq. (2.31) with $t^{\text{eff}} = \langle t \rangle$. Although the ATA1 and ATA2 defined in this way for momentum density carry the spirit of the corresponding versions of the ATA used for densities of states in Ref. 3, they are not strictly equivalent to those.

[16]In contrast, the Bloch spectral density in ATA1 and ATA2 shows pronounced differences associated with the impurity states (see Fig. 2 of Ref. 3).

[17]The present calculations on $Cu_{0.75}Ni_{0.25}$ employ the same Ni potential as Ref. 2. The Ni potential for $Cu_{0.5}Ni_{0.5}$ and $Cu_{0.25}Ni_{0.75}$, however, differs slightly from that used in Ref. 2 in that the Ni $3d$ resonance is higher in energy by 0.03 Ry. (This Ni potential was used extensively in Refs. 3–5.) The Cu potential used in all the computations reported in this article is identical to that of Ref. 2. Concerning other details of the calculations, we note that our programs require on the order of one minute of CPU time on Cyber 72 computer to carry out one iteration of the CPA equation. (The total CPU time, of course, depends upon the number of energies one considers and the accuracy one wants.) Finally, numerical interpolation in energy was used in computing KKR structure functions, as in Ref. 3.

[18]In expansion (A7), $\vec{r}$ is assumed to be confined to the Wigner-Seitz cell at the site $m \neq n$. This expansion does not hold for arbitrary crystal structures, although it can be shown to be valid for close-packed lattices.

[19]See Appendix A of Ref. 1.